Unprecedented palladium(II) complex containing dipodal 1,3,4-thiadiazole derivatives: synthesis, structure, and biological and thermal investigations†

Leila Heidari,[a] Mitra Ghassemzadeh,*[a] Dieter Fenske,[b] Olaf Fuhr,[b] Maryam Saeidifar[c] and Farshid Mohsenzadeh[a]

A novel mononuclear palladium(II) complex, [Pd(**L**)Cl_2] DMF (**1**·DMF, **L** = 1,4-bis(5-amino-1,3,4-thiadiazol-2-sulfanyl-methyl)benzene), has been synthesized and characterized by elemental analysis, FT-IR and ^{1}H NMR spectroscopy and single-crystal X-ray diffraction. On the basis of the molecular structure, in **1**·DMF, a ligand acts as a bidentate chelating one using its endocyclic nitrogen atoms. The biological activities of the free ligand and its palladium complex including cytotoxic activity towards the human colon cancer cell line (HCT-116) and antibacterial activity against one Gram-negative strain (*Escherichia coli* (ATCC 25922)) and one Gram-positive strain (*Staphylococcus aureus* (ATCC 6538)) have been examined. The IC_{50} value of **1**·DMF against HCT-116 was 500 μM, which is much higher than that reported for cisplatin, and hence, the compound exhibited low anticancer efficacy compared to cisplatin. However, it exhibited excellent antibacterial activities against both Gram-negative as well as Gram-positive bacterial microorganisms. Furthermore, the thermal stability of complex **1**·DMF was studied by thermal gravimetric analysis (TGA). The resulting product was characterized as highly pure PdO nanoparticles (mean crystallite size: 39 nm) by using a series of techniques including powder XRD, EDAX, and SEM.

1. Introduction

1,3,4-Thiadiazole and its derivatives as nitrogen–sulfur heterocycles are of great interest due to their peculiar properties and broad spectrum of applications in various areas of science, *e.g.*, chemistry, biology, agriculture, and medicine. During the past few decades, the synthesis, properties, and applications of 1,3,4-thiadiazoles have been the subject of numerous reviews and book chapters.[1–7]

From a chemistry viewpoint, 1,3,4-thiadiazole ring systems – consisting of two nitrogen atoms, one sulfur atom and two double bonds – undergo various substitution reactions to afford 2,5-disubstituted derivatives. As shown in Scheme 1, derivatives of 2-mercapto-1,3,4-thiadiazole, especially 5-amino-2-mercapto-1,3,4-thiadiazole, generally exhibit thiol–thione or amino–imino tautomerism in a solution, which may enhance their reactivity in substitution reactions and their ability in the formation of metal complexes.

Therefore, 5-substituted-2-mercapto-1,3,4-thiadiazoles display different bonding possibilities due to the multiple "hard" (exo- and endocyclic nitrogen atoms) and "soft" (exocyclic sulfur atom) donor sites (Scheme 2). Depending on the nature of the metal ion, they may act as monodentate N- or S-ligands (forms I and II),[8–12] N,S bidentate chelating or bridging ligands (forms III and IV),[13,14] *N*,*N*′-bidentate bridging ligands (form V)[15,16] and S-bridging ligands (form VI)[17] leading to the formation of mono-, bi- or multinuclear metal complexes.

Among nitrogen and sulfur donor heterocycles, substituted 1,3,4-thiadiazole derivatives and their corresponding metal complexes have been increasingly utilized as pharmaceuticals because of their interesting biological activities, including antimicrobial,[18,19] antituberculosis,[20] antiviral,[21] antifungal,[22,23]

[a] *Department of Inorganic Chemistry, Chemistry & Chemical Engineering Research Center of Iran, Pajoohesh Blvd., 17th Km of Tehran Karaj Highway, Tehran 14968 13151, Iran. E mail: mghassemzadeh@ccerci.ac.ir; Fax: +98 21 44787753; Tel: +98 21 44787706*

[b] *Institut fur Nanotechnologie and Karlsruhe Nano Micro Facility (KNMF), Karlsruher Institut fur Technologie, Hermann von Helmholtz Platz 1, Eggenstein Leopoldshafen 76344, Germany*

[c] *Department of Nanotechnology and Advanced Materials, Materials and Energy Research Center, Karaj, Iran*

† Electronic supplementary information (ESI) available: Experimental details for the preparation of 1,4 bis(5 amino 1,3,4 thiadiazol 2 sulfanyl methyl)benzene (**L**). Spectroscopic data of **L** and **1**·DMF. Additional figures (antibacterial activities, XRD, EDX, and SEM). CCDC 2006283. For ESI and crystallographic data in CIF or other electronic format see DOI: 10.1039/d0nj02918a

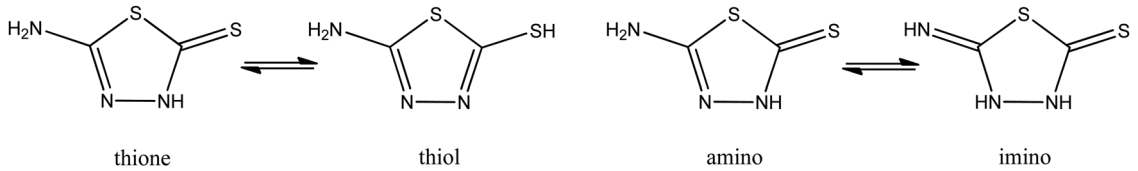

Scheme 1 Thio thione or amino imino tautomerism in 5 amino 2 sulfanyl 1,3,4 thiadiazole.

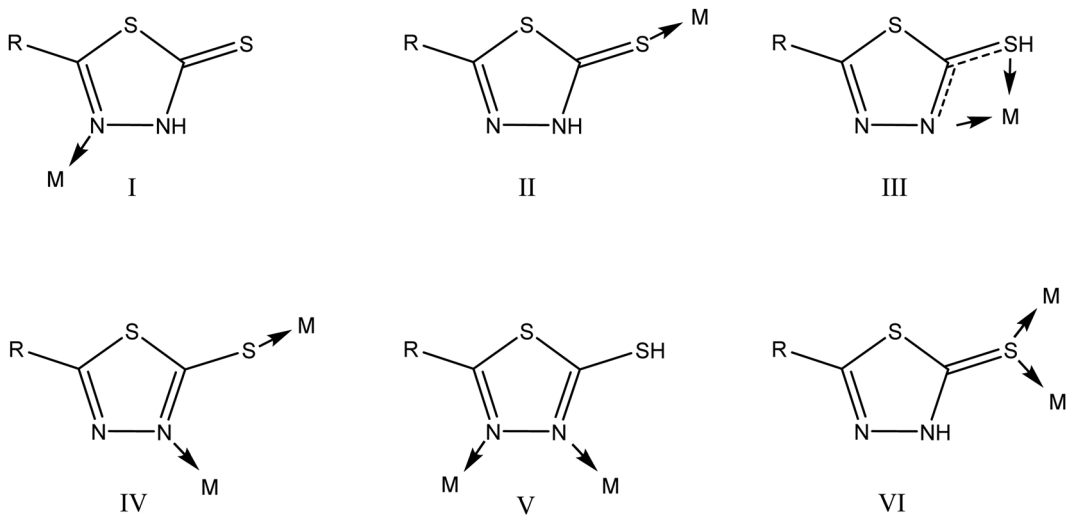

Scheme 2 Possible coordination modes of 5 substituted 2 mercapto 1,3,4 thiadiazole.

analgesic,[24] antidepressant and anxiolytic.[25,26] In general, these activities are attributed to the presence of the toxophoric >NCS group and the strong aromaticity in the thiadiazole ring system caused by its two double bonds.[18,27]

In recent years, transition metal complexes containing organic N-, S-, O- and P donor ligands have been increasingly used as precursors for the synthesis of well-defined inorganic nanomaterials due to their convenient preparation under mild reaction conditions, excellent reproducibility, and high product quality.[28] Recently, we have reported the synthesis of some late transition metal complexes based on bis-(3-mercapto-1,2,4-triazole) and pyrazole derivatives and their application as precursors for the fabrication of the corresponding nano-scaled metals or metal oxides.[29–31] Moreover, we have found that the nanostructured materials can be produced from coordination compounds in the absence of any surfactant since the ligands (1,2,4-triazole and pyrazole derivatives) may act as capping agents. However, to the best of our knowledge, only a few articles deal with the preparation of these nanoparticles from palladium coordination compounds.[32]

Continuing our ongoing interest in the chemistry of nitrogen and sulfur heterocycles and their behavior towards late transition metal ions,[33–35] herein, we wish to report the synthesis and molecular structure of the first palladium complex containing 1,4-bis(5-amino-1,3,4-thiadiazol-2-sulfanyl-methyl)benzene. Due to notable biological activities of 1,3,4-thiadiazoles and their complexes, we primarily assessed the anticancer and antibacterial activities of the synthesized complex. Since such coordination complexes have the potential to be a suitable precursor for metal-based nanomaterials,[28] the thermal behavior of the synthesized complex was also explored and the chemical nature, morphology, and size of the final product (upon pyrolysis) were elucidated.

2. Results and discussion

2.1. Synthesis and characterization of 1·DMF

Complex **1**·DMF can be obtained through the reaction of **L** (ESI†) with palladium(II) chloride in a molar ratio of 1 : 1 in dimethylformamide/acetonitrile in excellent yield as a yellowish air-stable solid mass (Scheme 3).

In the ^{1}H NMR spectrum of **1**·DMF in DMSO (Fig. SF4, ESI†), the signals of the protons of S–CH_2 moieties and the aromatic ring can be observed as multiplets at δ = 4.08–4.39 and 6.90–7.37, respectively. The signal at δ = 7.38 ppm for one proton and the multiplets at δ = 8.39–9.03 for three protons are due to the NH_2 protons that are exchangeable by D_2O (Fig. SF5, ESI†). The splitting of the signals to multiplets with respect to those in the free ligand (ESI†) indicates that the ligand occurs in a non-symmetric mode in the complex. Furthermore, the ^{1}H NMR spectra include three signals at δ = 7.95, 2.89, and 2.73 ppm assignable to the CHO group and two methyl moieties of the DMF molecule in the complex. The FT-IR spectra of **1**·DMF show two bands at 3106 cm^{-1} and 3169 cm^{-1}, which can

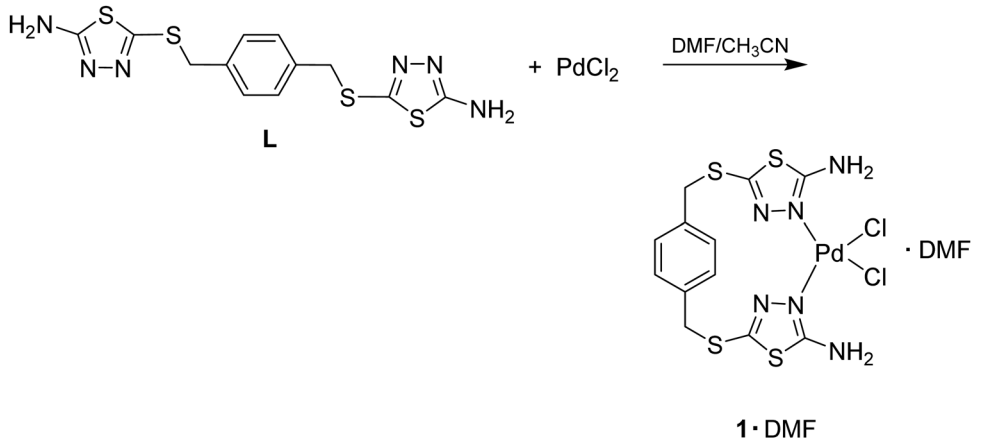

Scheme 3 Synthesis route of **1**·DMF.

be assigned to the valence vibrations of NH bonds of the NH_2 moieties (Fig. SF6, ESI†). Moreover, the C N and C–S vibrations can be observed at 1651 and 723 cm^{-1}. Besides, the Far-IR spectrum of **1**·DMF exhibits two absorption bands at 277 and 327 cm^{-1}, which can be ascribed to the Pd–Cl and Pd–N vibrations, respectively (Fig. SF7, ESI†).

2.2. Crystal structure analysis of complex 1·DMF

Crystallographic data and selected bond distances and angles are given in Tables 1 and 2, respectively. According to the crystallographic data, the complex crystallizes in the monoclinic $P2_1/c$ space group. Complex **1**·DMF consists of one neutral palladacycle, [Pd(**L**)Cl_2] (**1**), along with one solvent molecule DMF (Fig. 1).

According to the determined molecular structure, the bitopic ligand acts as a bidentate one and coordinates to the metal center through nitrogen atoms (N2 and N5) of the two heterocycles in a *cis* fashion. The square planar coordination around the metal center is completed by two chlorine atoms (Fig. 1, Cl1–Pd1–Cl2: 91.39(2)°, N2–Pd1–Cl1: 89.90°, N5–Pd1–Cl2: 89.69° and N5–Pd1–N2: 89.42°). The Pd–N- and Pd–Cl bond lengths (meanly 2.02 Å and 2.29 Å, respectively) are in good agreement with the range observed in other *cis*-dichloropalladacycles containing nitrogen donor ligands.[36,37]

Furthermore, the solvent molecule acts as a bridging agent between two 1,3,4-thiadiazole rings. It links their NH_2 groups through its oxygen atom (O1) *via* medium-strong hydrogen bondings (N6···O1 : 2.96(2) Å, N6–H6A···O1 : 171.4(3)°, N1···O1 : 2.84(2) Å, and N1–H1A···O1 : 169.8(3)°) and may be responsible for further stabilization of the complex (Fig. 1).

Furthermore, the dihedral angles between the ''best planes'' of the benzene ring and the heterocycles (A: C1, S1, N2, N3, C2), (B: S4, C11, N4, N5, C12) and (C: C8, C7, C6, C5, C4, C9) are 42.12 (6)° (A and C) and 45.37 (7)° (B and C). Moreover, the two heterocycles coordinating to palladium atoms are tilted by 85.23° with respect to each other.

The crystallographic data have been deposited with the Cambridge Crystallographic Data Centre (CCDC) as supplementary publication number CCDC 2006283 (**1**·DMF).†

Table 1 Crystal data and structure refinement for **1**·DMF

Emp. formula	$C_{15}H_{19}Cl_2N_7OPdS_4$
Formula mass	618.91
Crystal size [mm]	0.24 × 0.05 × 0.04
Crystal system	Monoclinic
Space group	$P2_1/c$
a [Å]	8.138(1)
b [Å]	23.012(4)
c [Å]	12.305(2)
α [°]	90
β [°]	96.063(1)
γ [°]	90
Volume [Å^3]	2291.7(6)
Z	4
D_{calcd} [g cm ^{3}]	1.794
Absorp. correct.	
μ [cm ^{1}]	8.184
F(000)	1240.0
Temp. [K]	180.2
2Θ range for data collection/°	6.68 to 124.99
Index range	
h	10 → 10
k	30 → 30
l	16 → 8
Reflect. collected	23 896
Radiation	Ga K_α (λ 1.34143)
Uniq. reflect. (R_{int}, R_{Sigma})	5473 (0.0173, 0.0119)
Reflect. with $I \geq 2\sigma$ (I)	5062
Parameters	347
Goodness of fit on F^2	1.024
Final R indexes [$I \geq 2\sigma$ (I)]	R_1 0.0279, wR_2 0.0756
Final R indexes [all data]	R_1 0.0301, wR_2 0.0770[a]
Largest diff. peak/hole/e Å ^{3}	0.80/ 1.03
CCDC number	2006283

[a] w $1/[\sigma^2(F_o^2) + (0.0476P)^2 + (1.8570P)]$; P $[\max(F_o^2, 0) + 2F_c^2]/3$.

Table 2 Selected bond distances [Å] and bond angles [°] of **1**·DMF

Pd1 Cl1	2.281(6)	S3 C10	1.842(3)	Cl1 Pd1 Cl2	91.39(2)
Pd1 Cl2	2.301(6)	S3 C11	1.746(2)	N2 Pd1 Cl1	89.80(6)
Pd1 N2	2.017(2)	S4 C11	1.745(3)	N2 Pd1 Cl2	174.06(6)
Pd1 N5	2.015(2)	S4 C12	1.735(2)	N5 Pd1 Cl1	176.91(6)
S1 C1	1.735(2)	C13 O1	1.235(3)	N5 Pd1 Cl2	89.69(6)
S1 C2	1.734(3)	C13 N7	1.324(3)	N5 Pd1 N2	89.42(8)
S2 C2	1.753(2)	C14 N7	1.457(4)	C2 S2 C3	98.18(1)
S2 C3	1.842(3)	C15 N7	1.447(4)	C11 S3 C10	100.01(1)

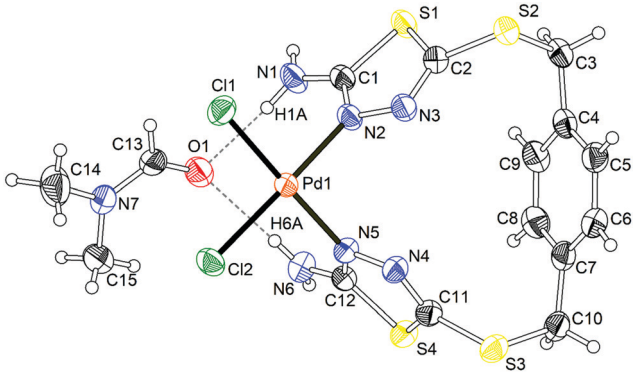

Fig. 1 Molecular structure of **1**·DMF (thermal ellipsoids are depicted at the 50% probability level), showing the hydrogen bondings between NH_2 moieties and DMF.

2.3. *In vitro* cytotoxicity studies

2.3.1. Cell viability assay. The cytotoxicity evaluation of **L** and **1**·DMF against the HCT-116 cell line (Fig. 2) showed that the increase in their concentration reduced the cell viability percentage; hence, the cancer cell line viability of the tested compounds turned out to be dose-dependent. The IC_{50} of complex **1**·DMF is 500 μM, while it was 1000 μM for **L**. The results revealed that the effectiveness of the complex was higher than the free ligand. However, **1**·DMF displayed poor anticancer activity and remained ineffective against the test cell lines with respect to the other palladium complexes (18.09 μM,[38] 119.0 μM[39] and 100 μM[40]) and cisplatin (5.18 μM[41] and 23.92 μM[42]) as a standard anticancer drug. Therefore, **1**·DMF was not found to be a suitable candidate for an anticancer drug.

2.3.2. Morphological assessments. The DAPI stained morphologically normal nuclei blue having round shape, and sharp edges are shown in the control groups (Fig. 3), leading to a significant increase in rounded cells in **L** and complex **1**·DMF groups. Consequently, it was clearly observed that apoptotic cells were increased due to the presence of deformed and fragmented nuclei with condensed chromatin in the **L** or **1**·DMF groups (shown with arrows). In addition, the apoptotic cells in the complex **1**·DMF groups were more than in the **L** groups. Consequently, cancer cell death in the complex **1**·DMF groups was greater than in the ligand groups indicating more effectiveness of complex **1**·DMF. This result was in agreement with MTT assay results.

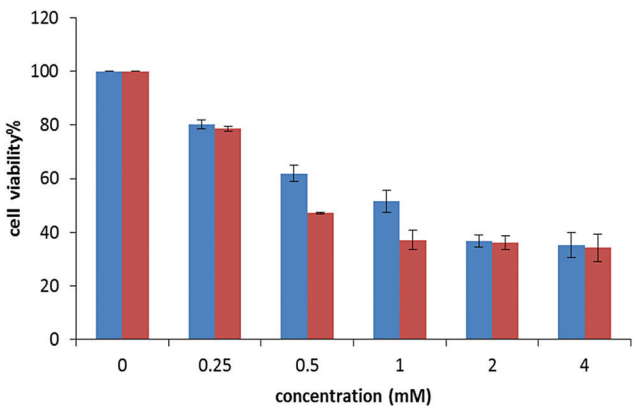

Fig. 2 Cell viability percentage of HCT 116 with increasing concentration of **L** (blue), and complex **1**·DMF (red).

2.3.3. Antibacterial activity. The antibacterial activity of the ligand and its palladium(II) complex was tested *in vitro* against two pathogenic bacterial strains involving one Gram-negative (*Escherichia coli* ATCC 25922, PTCC 1399) and one Gram-positive bacterial strain (*Staphylococcus aureus* ATCC 6538, PTCC 1112). The bacterial suspensions treated with the ligand, its palladium complex along with the ligand- and complex-free control samples after cultivation (r.t., 24 h) and incubation (37 °C, 24 h) are presented in Fig. SF8 and SF9 (ESI†). The results of the biological investigations are summarized in Table ST1 (ESI†). According to the test results, the complex exhibits excellent antibacterial activity towards Gram-negative as well as Gram-positive bacterial strains, since almost no bacterial colonies could be observed in the cultures treated with the complex after cultivation and incubation for all the dilutions (Fig. SF8c and SF9c, ESI†). Yet, the ligand displays higher activity against Gram-negative bacterial strains than against Gram-positive ones. The rates of antibacterial activity against Gram-negative bacterial strains of 99.93% for **1**·DMF and 99.33% for **L** indicate that the ligand and its palladium complex show similar strong biological effects towards this microorganism. This is while the antibacterial rates of the test samples against Gram-positive bacteria were found to be 99.33% for **1**·DMF and 84% for **L**, which represents an increase in the antibacterial potency of the ligand after coordination to the metal ion.

2.4. Thermal gravimetric analysis

The thermal stability of the complex has been studied using the thermal gravimetric analysis technique (TGA). The TG curve of the complex undergoes a decomposition process over three stages (Fig. 4). The initial weight loss from ambient temperature to 230 °C is associated with the removal of one DMF molecule along with the two NH_2 groups of the ligand (found: 13.9%; calc.: 14%). The observed weight loss in the temperature region of 230 °C to 317 °C is related to the removal of two halide ions (found: 11.2%, calc.: 11%). Finally, the last thermal decomposition occurs in the temperature range of 317–450 °C, which could be attributed to the total decomposition of the ligand (found: 54.9%, calc.: 54.3%). The TG analysis of **1**·DMF revealed that the final product of the thermal decomposition of the complex at 600 °C is PdO (found: 19.93%, calc.: 19.7%). In order to determine the chemical and morphological structure of the final product from the TG analysis, the resulting material (sample) was analyzed *via* X-ray powder diffraction (XRD), scanning electron microscopy (SEM) and energy-dispersive X-ray spectroscopy (EDX). The sharp diffraction peaks observed in the powder XRD pattern of the sample (Fig. SF10, ESI†) indicate a high crystallinity of the sample. The XRD pattern shows solely the reflections from the (101), (110), (112), (103), (200), (004) and (211) diffraction

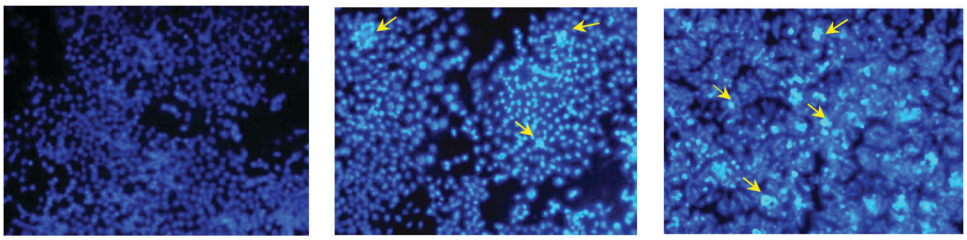

Fig. 3 DAPI staining of (a) control, (b) **L**, and (c) complex **1**·DMF onto treated HCT 116.

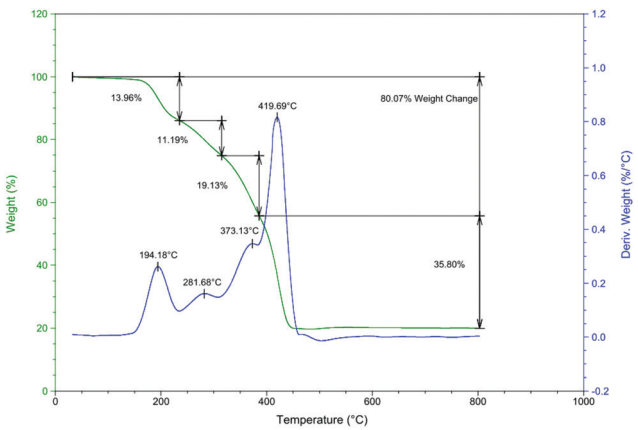

Fig. 4 TGA curve of complex **1**·DMF.

planes, which are characteristic of the PdO phase (JCPDS-No. 411107) and confirm its phase purity. The EDX analysis shows the presence of the elements palladium and oxygen, which also confirmed the formation of PdO (Fig. SF11, ESI†). The morphology of the resulting compound was determined *via* scanning electron microscopy (SEM). The SEM image of the product obtained from the thermolysis of **1**·DMF revealed the formation of PdO nanoparticles (Fig. SF12, ESI†). The mean crystallite size for the PdO nanoscaled material was determined from the Debye–Scherrer equation and was found to be 39 nm.[43]

3. Conclusions

In this report, a novel palladium(II) complex containing dipodal bis-1,3,4-thiadiazole-based ligands has been introduced. The molecular structure of complex **1**·DMF revealed that ligand **L** coordinates to the palladium(II) chloride moiety using its endocyclic hydrazinic nitrogen atoms of the 1,3,4-thiadiazole system in a *cis* fashion.

The screening of ligand **L** and complex **1**·DMF against two bacterial pathogens (a Gram-positive bacterial strain (*Staphylococcus aureus*) and a Gram-negative bacterial strain (*Escherichia coli*)) and human colon cancer cell lines (HCT-116) was carried out. The results revealed that the cancer cell line viability of **L** and **1**·DMF was dose-dependent and showed cytotoxic activity against the tested cell lines lower than cisplatin, while they exhibited very high to excellent antibacterial activities.

The thermal investigations indicated that the complex decomposes at about 600 °C resulting in the formation of uniform, pure palladium(II) oxide nanoparticles (mean crystallite size of 39 nm). The nature, chemical composition, and morphology of the produced nanostructure were thoroughly studied using various techniques.

This novel bioactive complex may be a promising candidate for pharmaceutical applications due to its interesting antibacterial properties. Besides, this coordination complex may be considered as a useful surrogate to other precursors for the fabrication of the palladium(II) oxide nanostructure.

4. Experimental section

4.1. Materials and instruments

All reagents and solvents were purchased from Merck and Fluka and used without further purification. The microorganisms used in this study were obtained from the microorganism bank of the Iranian Biological Resource Center.

FT-IR spectra were recorded as KBr discs (4000–400 cm^{-1}) or Nujol mulls (CsI cells 500–200 cm^{-1}) using a PerkinElmer 400 spectrometer. The ^1H NMR spectra were recorded on a Bruker-AQS AVANCE 300 MHz spectrometer using TMS (δ = 0.0 ppm) as an internal standard. LC/MS-API was recorded on an alliance 2695 system. Elemental analyses (C, H, and N) were performed on an Elementar Vario EL III elemental analyzer. Thermogravimetric analysis (TGA) was performed on a Mettler-Toledo TGA/SDTA 851e thermal analyzer in a flowing air atmosphere at a heating rate of 10 °C min^{-1} from 25 to 800 °C. The powder X-ray diffraction measurements were carried out using an X'PERT-PRO diffractometer with a Cu anode that generated Cu K_α radiation, λ = 1.5406 Å.

4.2. Synthesis of complex 1·DMF

To a hot solution of **L** (0.1 g, 0.27 mmol) in DMF (10 mL) was added a hot solution of $PdCl_2$ (0.048 g, 0.27 mmol) in CH_3CN (10 mL) under stirring and the resulting mixture was stirred for 24 h. The completion of the reaction was monitored by TLC, using *n*-hexane : ethyl acetate : ethanol (5 : 3 : 1) as an eluent. The yellow precipitate was filtered, washed with DMF and CH_3CN (10 mL for each solvent) and air dried. Yield: 0.15 g

(90%), mp: 285 °C (dec.); elemental calculations for $C_{15}H_{19}Cl_2N_7OPdS_4$ (618.94): C, 29.11; H, 3.09; N, 15.84. Found: C, 29.18; H, 2.94; N, 15.45%. FT-IR (KBr, ν, cm^{-1}): 3403 (m), 3366 (m), 3253 (m, ν_{N-H}), 3169 (m, ν_{N-H}), 2969 (w), 2731 (w), 1643 (s), 1618 (s, $\nu_{C\ \ N}$), 1513 (s), 1422 (m), 1388 (w), 1346 (w), 1246 (w), 1096 (s), 1025 (m), 888 (w), 833 (w), 779 (w), 662 (w, ν_{C-S}), 633 (w), 558 (w), 475 (w). FT-IR (Nujol mull, ν, cm^{-1}): 327 (m, ν_{Pd-N}), 277 (m, ν_{Pd-Cl}). ^{1}H NMR (δ, DMSO-d_6, 500 MHz): 8.4–9.03 (m, 3H, NH_2, exchangeable with D_2O), 7.95 (s, 1H, CH_{DMF}), 7.38 (s, 1H, NH_2, exchangeable with D_2O), 6.90–7.35 (m, 4H, CH Ar), 4.08–4.39 (m, 4H, CH_2S), 2.73 and 2.89 (s, 6H, CH_{3DMF}).

4.3. Crystal structure analysis of complex 1·DMF

The selected crystal of **1**·DMF was covered with perfluorinated oil and mounted on a STOE StadiVari single-crystal diffractometer (Ga K_α radiation with λ = 1.34143 Å). The orientation matrix and the unit cell dimensions were determined from 30 375 reflections. Using Olex2,[44] the structure was solved with the ShelXT[45] structure solution program using Intrinsic Phasing and refined with the ShelX[46] refinement package using Least Squares minimization. All non-hydrogen atoms were refined with anisotropic displacement parameters; hydrogen atoms could be localized and were refined freely.

4.4. *In vitro* cytotoxic assay

4.4.1. MTT assay. The MTT assay was performed on human colon cancer cell lines, HCT-116, for the evaluation of cell viability of **L** and complex **1**·DMF. For this purpose, plates of 96 wells were filled with 100 μL culture medium containing 5×10^3 seeded cells and incubated at 37 °C for 24 h. After medium removal, the cells were treated with the above two compounds in the range of 0–4 mM for 72 h. 10 μL of MTT solution (5 mg mL^{-1} in RPMI-1640 without phenol red) was then added to each well and incubated in darkness at 37 °C for 4 h to form formazan crystals. Finally, the media were removed, and the formazan crystals were dissolved by the addition of DMSO (100 μL). The absorbance of the supernatant solution was recorded after 20 min at 570 nm using a Microplate Reader (Biotek, USA). Cell viability percentage was determined as follows:

$$\text{Cell viability} = (OD_{treated}/OD_{control}) \times 100\%$$

where $OD_{treated}$ and $OD_{control}$ are the optical densities of the treated cells and untreated cells, respectively.

4.4.2. DAPI staining. DAPI is a blue fluorescent probe that fluoresces brightly upon selective binding to the minor groove of double-stranded DNA, where its fluorescence is approximately 20-fold greater than in the non-bound state.[47] DAPI staining can be demonstrated by apoptotic induction and nuclear change of cancer cell lines treated with the drug candidate. In this experiment, the colon cancer cell lines HCT-116 were seeded in 6-well plates. After the cells reached the desired density, they were treated with IC_{50} of the ligand (1000 μM) and complex **1**·DMF (500 μM) for 72 h, separately.[48] The wells were then washed with PBS and fixed with methanol for 20 min at room temperature and washed once more with PBS. The DAPI solution (1 μg mL^{-1}) was added to each well of cells and was left for 10–60 s. Then, the unincorporated DAPI solution was removed, and the wells were washed with PBS. Finally, the wells were observed using a fluorescence microscope.

4.4.3. *In vitro* antibacterial assay. The antibacterial behavior of the ligand and its palladium complex against two bacterial strains was evaluated using the plate colony-counting method. In order to determine the rate of bacterial growth, bacterial suspensions of *Staphylococcus aureus* (ATCC 6538, PTCC 1112) and *Escherichia coli* (ATCC 25922, PTCC 1399) were prepared using the direct colony method, where the colonies were taken directly from the plate of fresh-cultivated bacteria and were suspended in sterile 0.9% normal saline. Then, these initial suspensions were adjusted to match the turbidity of a 0.5 McFarland standard (corresponding to the 1.5×10^8 colony forming units (CFU) per mL using 0.05 mL 1.175% w/v $BaCl_2 \cdot 2H_2O$ + 99.5 mL 1% w/v H_2SO_4). The initial suspensions were then 10-fold serially diluted (up to 10^{-2}) in saline (0.9%). The resulting suspension with a concentration of 1.5×10^6 CFU per mL was also used as the control sample (blank sample). On the other hand, the solutions of the ligand and its palladium complex in dimethyl sulfoxide (5 mM) were prepared by dissolving the ligand (3.68 g, 10 mmol) in DMSO (2 mL) and **1**·DMF (6.19 g, 10 mmol) in DMSO (2 mL) and used as test substances. The bacterial suspensions (2 mL) were next spread over the surface of nutrient agar plates containing the test substances (0.5 mL). The plates were incubated at ambient temperature for 24 h. After incubation for 24 h at 37 °C, the samples were 10-fold serially diluted in saline (up to 10^{-5}). 1 mL of each dilution was transferred to agar plates. The number of surviving bacterial colonies (measured in CFUs) was quantitated after cultivation at ambient temperature for 24 h and subsequent incubation of the plates at 37 °C for 24 h. The rates of colony-forming units (R) were calculated considering the dilution factor using the following equation:

$$R = [(N \text{ control} \quad N \text{ sample})/N \text{ control}] \times 100\%$$

where N control and N sample represent the average number of bacterial colonies of the control sample (containing no antibacterial agent), and ligand- and complex-test samples, respectively. All the tests were performed in triplicate.

Conflicts of interest

There are no conflicts to declare.

Acknowledgements

This work was partly carried out with the support of the Karlsruhe Nano Micro Facility (KNMF), a Helmholtz Research Infrastructure at KIT, and the authors would like to thank Sven Stahl for his assistance with the analyses.

References

1 A. Abdildinova and Y.-D. Gong, *ACS Comb. Sci.*, 2018, **20**, 309–329.
2 G. Serban, O. Stanasel, E. Serban and S. Bota, *Drug Des., Dev. Ther.*, 2018, **12**, 1545–1566.
3 J. Dwivedi, N. Kaur, D. Kishore, S. Kumari and S. Sharma, *Curr. Top. Med. Chem.*, 2016, **16**, 2884–2920.
4 Y. Hu, C.-Y. Li, X.-M. Wang, Y.-H. Yang and H.-L. Zhu, *Chem. Rev.*, 2014, **114**, 5572–5610.
5 M. Yusuf and P. Jain, *Arabian J. Chem.*, 2014, **7**, 525–552.
6 A. K. Jain, S. Sharma, A. Vaidya, V. Ravichandran and R. K. Agrawal, *Chem. Biol. Drug Des.*, 2013, **81**, 557–576.
7 Y.-J. Wu, Five-Membered Ring Systems: With N and S Atom, *Progress in Heterocyclic Chemistry*, 2017, ch. 5.5, vol. 29, pp. 315–336.
8 Y. Ma, B. Mu and R.-D. Huang, *Transition Met. Chem.*, 2018, **43**, 103–113.
9 G. E. Camí, M. Liu González, F. Sanz Ruiz and J. C. Pedregosa, *J. Phys. Chem. Solids*, 2005, **66**, 936–945.
10 D. Varna, E. Kapetanaki, A. Koutsari, A. G. Hatzidimitriou, G. Psomas, P. Angaridis, R. Papi, A. A. Pantazaki and P. Aslanidis, *Polyhedron*, 2018, **151**, 131–140.
11 P. Bharati, A. Bharti, P. Nath, S. Kumari, N. K. Singh and M. K. Bharty, *Inorg. Chim. Acta*, 2016, **443**, 160–169.
12 B.-C. Tzeng, G.-H. Lee and S.-M. Peng, *Inorg. Chem. Commun.*, 2004, **7**, 151–154.
13 L. Li, L. Wei, X. Si, L. Fan, C. Wang and H. Hou, *Inorg. Chim. Acta*, 2013, **405**, 279–287.
14 S. A. Al-Jibori, E. G. H. Al-Saraj, N. Hollingsworth and G. Hogarth, *Polyhedron*, 2012, **44**, 210–214.
15 P.-Z. Hu, J.-G. Wang, L.-F. Ma, J.-H. Qin, B.-T. Zhao and L.-Y. Wang, *J. Mol. Struct.*, 2008, **876**, 225–233.
16 J.-L. Song, Z.-C. Dong, H.-Y. Zeng, W.-B. Zhou, T. Naka, Q. Wei, J.-G. Mao, G.-C. Guo and J.-S. Huang, *Inorg. Chem.*, 2003, **42**, 2136–2140.
17 F. Karasmani, A. Tsipis, P. Angaridis, A. G. Hatzidimitriou and P. Aslanidis, *Inorg. Chim. Acta*, 2018, **471**, 680–690.
18 E. Yousif, A. Majeed, K. Al-Sammarrae, N. Salih, J. Salimon and B. Abdullah, *Arabian J. Chem.*, 2017, **10**, S1639–S1644.
19 Y. Cheng, Q. Feng, M. Yin, X. Ren, J. Wang and Y.-H. Zhou, *New J. Chem.*, 2016, **40**, 9125–9131.
20 E. E. Oruc, S. Rollas, F. Kandemirli, N. Shvets and A. Dimoglo, *J. Med. Chem.*, 2004, **47**, 6760–6767.
21 X. Gan, D. Hu, Z. Chen, Y. Wang and B. Song, *Bioorg. Med. Chem. Lett.*, 2017, **27**, 4298–4301.
22 Y. I. El-Gazzar, H. H. Georgey, S. M. El-Messery, H. A. Ewida, G. S. Hassan, M. M. Raafat, M. A. Ewida and H. I. El-Subbagh, *Bioorg. Chem.*, 2017, **72**, 282–292.
23 P. Zoumpoulakis, C. Camoutsis, G. Pairas, M. Soković, J. Glamočlija, C. Potamitis and A. Pitsas, *Bioorg. Med. Chem.*, 2012, **20**, 1569–1583.
24 S. Schenone, C. Brullo, O. Bruno, F. Bondavalli, A. Ranise, W. Filippelli, B. Rinaldi, A. Capuano and G. Falcone, *Bioorg. Med. Chem.*, 2006, **14**, 1698–1705.
25 M. Yusuf, R. A. Khan and B. Ahmed, *Bioorg. Med. Chem.*, 2008, **16**, 8029–8034.
26 F. Clerici, D. Pocar, M. Guido, A. Loche, V. Perlini and M. Brufani, *J. Med. Chem.*, 2001, **44**, 931–936.
27 B. S. Holla, K. N. Poorjary, B. S. Rao and M. K. Shivananda, *Eur. J. Med. Chem.*, 2002, **37**, 511–517.
28 B. I. Kharisov, O. V. Kharissova, J. J. Ruíz Valdés and V. M. Jiménez Pérez, *Synth. React. Inorg., Met.-Org., Nano-Met. Chem.*, 2010, **40**, 640–650.
29 S. Bahemmat, M. Ghassemzadeh and B. Neumüller, *Inorg. Chim. Acta*, 2015, **435**, 159–166.
30 S. Bahemmat, M. Ghassemzadeh, M. Afsharpour and K. Harms, *Polyhedron*, 2015, **89**, 196–202.
31 S. Bahemmat, B. Neumüller and M. Ghassemzadeh, *Eur. J. Inorg. Chem.*, 2015, 4116–4124.
32 Z. Sorinezami, H. Mansouri-Torshizi, M. Aminzadeh, A. Ghahghaei, N. Jamgohari and M. Heidari Majd, *J. Biomol. Struct. Dyn.*, 2019, **37**, 4238–4250.
33 M. Ghassemzadeh, M. Bolourtchian, S. Chitsaz, B. Neumüller and M. M. Heravi, *Eur. J. Inorg. Chem.*, 2000, 1877–1882.
34 M. Ghassemzadeh, S. Bahemmat, M. Mahmoodabadi, B. Rezaii-Rad, H. H. Monfared, E. Mottefakeri and B. Neumüller, *Polyhedron*, 2010, **29**, 3036–3045.
35 M. Ghassemzadeh, R. Firouzi, S. Shirkhani, S. Amiri and B. Neumüller, *Polyhedron*, 2014, **69**, 188–196.
36 N. Andrade-López, *Polyhedron*, 2007, **26**, 4825–4832.
37 D. Schweinfurth, *Inorg. Chim. Acta*, 2011, **374**, 253–260.
38 A. Savić, T. Marzo, F. Scaletti, L. Massai, G. Bartoli, R. Hoogenboom, L. Messori, R. Van Deun and K. Van Hecke, *Biometals*, 2019, **32**, 33–47.
39 E. H. Avdović, Ž. B. Milanović, M. N. Živanović, D. S. Šeklić, I. D. Radojević, L. R. Čomićd, S. R. Trifunović, A. Amić and Z. S. Marković, *Inorg. Chim. Acta*, 2020, **504**, 119465.
40 N. J. Patel, B. S. Bhatt, P. A. Vekariya, F. U. Vaidya, C. Pathak, J. Pandya and M. N. Patel, *J. Mol. Struct.*, 2020, **1221**, 128802.
41 A. R. Sayed, S. M. Gomha, E. A. Taher, Z. A. Muhammad, H. R. El-Seedi, H. M. Gaber and M. M. Ahmed, *Drug Des., Dev. Ther.*, 2020, **14**, 1363–1375.
42 M. P. Heng, Ch Tan, H. M. Saad, K. S. Sim and K. W. Tan, *Inorg. Chim. Acta*, 2020, **507**, 119581, DOI: 10.1016/j.ica.2020.119581.
43 A. L. Patterson, *Phys. Rev.*, 1939, **56**, 978–982.
44 O. V. Dolomanov, L. J. Bourhis, R. J. Gildea, J. A. K. Howard and H. Puschmann, *J. Appl. Crystallogr.*, 2009, **42**, 339–341.
45 G. M. Sheldrick, *Acta Crystallogr., Sect. A: Cryst. Phys., Diffr., Theor. Gen. Crystallogr.*, 2015, **71**, 3–8.
46 G. M. Sheldrick, *Acta Crystallogr., Sect. C: Cryst. Struct. Commun.*, 2015, **71**, 3–8.
47 J. Baharara, N. Hosseini and T. R. Farzin, *Cytotechnology*, 2016, **68**, 1403–1413.
48 N. Fattahian Kalhor, M. Saeidifar, H. Ramshini and A. A. Saboury, *J. Biomol. Struct. Dyn.*, 2020, **38**, 2546–2558.